Computational methodology for drug delivery to the inner ear using magnetic nanoparticle aggregates

Krzysztof Talaśka, Dominik Wojtkowiak, Dominik Wilczyński, Antoine Ferreira

Computational Methodology for Drug Delivery to the Inner Ear using Magnetic Nanoparticle Aggregates

Article *in* Computer Methods and Programs in Biomedicine · May 2022

DOI: 10.1016/j.cmpb.2022.106860

4 authors:

Krzysztof Talaśka
Poznan University of Technology
94 PUBLICATIONS **564** CITATIONS
SEE PROFILE

Dominik Wojtkowiak
Poznan University of Technology
51 PUBLICATIONS **297** CITATIONS
SEE PROFILE

Dominik Wilczyński
Poznan University of Technology
47 PUBLICATIONS **258** CITATIONS
SEE PROFILE

Antoine Ferreira
Institut National des Sciences Appliquées Centre Val de Loire
224 PUBLICATIONS **2,984** CITATIONS
SEE PROFILE

Computational Methodology for Drug Delivery to the Inner Ear using Magnetic Nanoparticle Aggregates

Krzysztof Talaśka , Dominik Wojtkowiak , Dominik Wilczyński , Antoine Ferreira

PII: S0169-2607(22)00242-5
DOI: https://doi.org/10.1016/j.cmpb.2022.106860
Reference: COMM 106860

To appear in: *Computer Methods and Programs in Biomedicine*

Received date: 13 December 2021
Revised date: 16 April 2022
Accepted date: 6 May 2022

Please cite this article as: Krzysztof Talaśka , Dominik Wojtkowiak , Dominik Wilczyński , Antoine Ferreira , Computational Methodology for Drug Delivery to the Inner Ear using Magnetic Nanoparticle Aggregates, *Computer Methods and Programs in Biomedicine* (2022), doi: https://doi.org/10.1016/j.cmpb.2022.106860

Computational Methodology for Drug Delivery to the Inner Ear using Magnetic Nanoparticle Aggregates

Krzysztof Talaśka *[1], Dominik Wojtkowiak [1], Dominik Wilczyński [1], and Antoine Ferreira *[2]

[1] Institute of Machine Design, Poznan University of Technology, Piotrowo 3, 61-138 Poznań, Poland,

[2] Laboratoire PRISME, Institut National des Sciences Appliquées (INSA) Centre Val de Loire, Bourges, France

Email: Krzysztof.talaska@put.poznan.pl and antoine.ferreira@insa-cvl.fr

* Corresponding authors

Graphical abstract

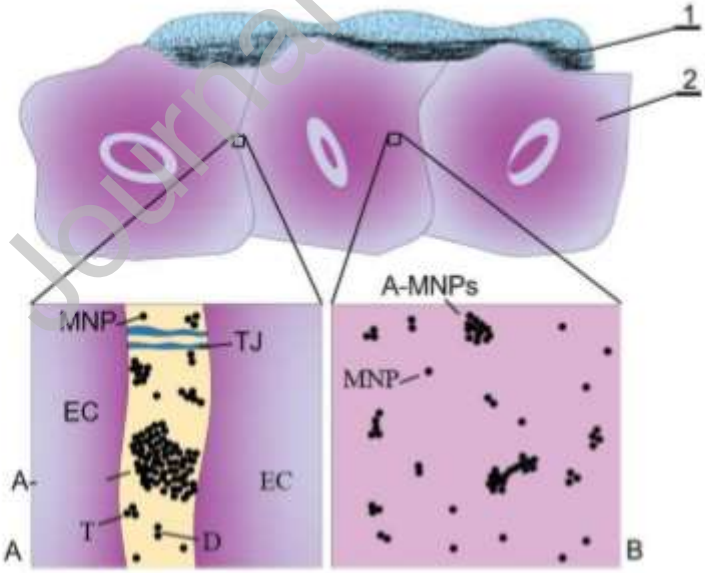

Computational methodology using Finite Element Modeling of the process of magnetic nanoparticles (MNPs) transport through the biological barrier (RWM)of the round windows membrane of inner ear.

HIGHLIGHTS

- The main goal of the proposed study is to improve the efficiency of the ear treatment by targeting drug delivery to the inner ear, namely the cochlea. Although drugs have been proposed to prevent damage or restore functionality to hair cells, a difficulty with such treatments is ensuring adequate drug delivery to the cells. To do so, we present a methodology for the evaluation of the magnetic forces needed to move magnetic particle nanorobots (termed MNPS) and their aggregates through the cochlea round window membrane (RWM). The presented finite element method can be an additional tool during the design of drug delivery systems to the inner ear using MNPs.

Abstract

Background and Objective: The main goal of the proposed study is to improve the efficiency of the ear treatment via targeted drug delivery to the inner ear, i.e. the cochlea. Although pharmacotherapy has been proposed as a solution to prevent damage or restore functionality to hair cells, the main challenge in such treatments is ensuring adequate drug delivery to the cells. To this end, we present a methodology for the evaluation of the magnetic forces needed to move magnetic particle nanorobots (abbreviated as MNP) and their aggregates through the cochlea round window membrane (RWM).

Methods: The FEM - Lagrangian-Eulerian approach (Abaqus software) was used to determine the specific parameters of movement of the nanoparticles crossing the RWM. This method results in a high consistency of FEM simulations and *in-vivo* experimental results in regards to the required magnetic force during the movement of spherical nanoparticles with a given viscosity η_{ave}. Based on the analysis of the experimental studies found in subject literature, the sizes of the MNPs and their aggregates able to cross RWM with and without the application of magnetic force F_M have been determined.

Results: The present work accounts for *b*oth the experimental and theoretical aspects of

these investigations. Presented research confirms the definite usability of the Lagrange-Euler method for the precise determination of the required magnetic force value *FM* to control the accelerated motion of MNP aggregates of complex shapes through RWM. It is possible to determine the predominant parameters with a precision of less than 5% for single-layer aggregates and spatial aggregates crossing the RWM. It can be concluded that the MNPs and their aggregates should not be larger than 500 nm — 750 nm to cross the RWM with high velocities of penetration close to 800 nm/s for magnetic forces of hundreds 10^{-14} Newtons.

Conclusions: The proposed Lagrangian-Eulerian approach is capable of accurately predicting the movement parameters of MNP aggregates of irregular shape that are close to the experimental test cases. The presented method can serve as a supplementary tool for the design of drug delivery systems to the inner ear using MNPs.

Keywords

Magnetic nanoparticles, aggregation design, drug delivery, inner ear, targeted therapy, Lagrange – Euler FEM analysis.

1. Introduction

Treating diseases of the inner ear is of particular interest for researchers, mainly due to the difficulty in delivering systemic drugs to the targeted location [1]. These problems derive from the presence of natural anatomical and physiological barriers [2]. This manifests itself particularly through the limited exchange of substances across the blood-perilymph barrier as well as the exchange between the plasma and the fluids of the inner ear [3]. Modeling techniques can lead to an improved design of fine, magnetic swimmers able cross the biological barriers and exert active control over the delivery of drugs to the inner ear. An analysis of the inner ear structure, in particular the cochlea, shows the following physical barriers separating the fluid in the cochlea from the inner ear and the circulatory system are: the oval window (OW), the blood inner ear barrier,and the round window membrane (RWM) [4]. What follows from such naturally occurring limitations for the delivery of pharmaceuticals to the cochlea, it is important to explore intelligent and non-invasive systems of targeted drug delivery to the desired location and in the exact amounts [5]-[7].

The current repertoire of drug delivery techniques include application either through the middle ear, to be deposited near the round window (intratympanic delivery), reliance of diffusion through the round window to reach the inner ear, or direct injection via the round window into the cochlea (intracochlear delivery), or via propulsion utilizing ultrasonic waves [8,9]. In the case of intratympanic delivery, a variety of methods are used in order to maintain contact with the membrane. Hydrogels can be used as carriers for drugs or micro/nanoparticles in order to extend contact time with the oval or round windows, as well as combinations thereof in the so-called ferrogels which can be manipulated through the use of magnetic fields. The most popular techniques employ nanoparticles as drug carriers [6]. Nanoparticles ranging from 10 nm to 200 nm in diameter can serve as an effective drug carrier [4],[10]-[13]. Placed near or directly on the surface of the physical barrier: RWM or OW, they are able to penetrate the barrier via the phenomenon of diffusion [4],[10]-[13]. RWM is

often used for analyzing the feasibility and potential of drugs delivery [4]. For the most part, this is the result of the manifested permeability of RWM [4],[10]-[13]. Out of all types of nanoparticles used to carry drugs to the cochlea, the methods employing magnetic nanoparticles (MNPs), also known as supermagnetic iron oxide NPs (SPIONs) show excellent potential for further development and application [2,4]. An external magnetic field enables to control the direction and velocity of MNPs in order to guide them to the desired location [14]. Depending on the MNP size, they can be channeled through blood vessels [15,16] or through selected body tissues [17]. It is important that the interaction of the MNPs and the external magnetic field can greatly accelerate the movement of the MNPs in its current medium [18]. Test results demonstrate a decided increase in the concentration of MNPs inside the cochlea (approximately 330%) under an active magnetic field in comparison to experiments carried out without the presence of an external magnetic field [13]. Scientific research of the last years confirms that this method is potentially useful for drug delivery to the cochlea [19,20]. An increasing number of articles present the results of experimental *in vivo* and *in vitro* studies in this area. They all clearly emphasize the advantage of magnetically active drug carriers (MNPs) in comparison to other types of NPs [4,13,18]-[20]. In addition to the experimental studies involving the methods of measuring movement time of MNPs through RWM, the visualization of this process, the determination of the magnetic field strength, the estimation of the magnetic push or pull force, a continuous pursuit of methods of designing systems enabling the delivery of MNPs to the cochlea is called for [4,13,18]-[20].

Advanced simulation methods based on the finite element method (FEM) can be of definite use in this matter, which already has been recognized in the research area covering MNPs delivery systems as well as the modelling of the inner ear, the cochlea and RWM [21]-[24]. We would like to propose a new and previously unused approach to determining the design parameters of the delivery system of the MNPs to the cochlea based on the numerical simulation analysis. The proposed FEM simulations are based on the Lagrangian-Eulerian approach, verified with selected

results of experimental studies, which is useful for determining the value of the magnetic force F_M needed to accelerate the movement of MNPs in a location such as the RWM tissue. Thus it becomes possible to determine the time necessary to move individual MNPs and their aggregates as well as to determine the relationship between the magnetic force F_M and the velocity v of the MNPs in the design process. This approach can be a successful complement of the research toolkit at the stage of designing and planning the application of MNPs in a new operating area.

2. Materials and Methods

When designing the delivery system for MNPs for transportation through RWM, several aspects call for a thorough analysis. Primarily, it is necessary to consider the complex structure of the RWM, the factors which affect its permeability and the complex phenomenon of aggregating individual MNPs in larger concentrations of particles for efficient drug delivery.

The research method presented in the present work is based on the use of numerical simulation methods. The simulation analyses conduced in this work employ the commercial software ABAQUS/Explicit. In order to develop the model for RWM, MNPs andtheir aggregates, the Lagrangian-Eulerian method was used. This method is used predominantly in the various analyses of the interaction between structural objects and liquids [21]. Its distinctive characteristics include the possibility to precisely calculate the forces acting on an object through a surrounding body as well as the ability to determine the object movement parameters within another body, making this method particularly usable for the analysis considering the interests presented in this work. For detailed information about the presented method, please refer to [48].

2.1. The anatomy of RWM

From the structural point of view, RWM is a three-layered membrane. From the side of the middle ear, one can distinguish the epithelium cell layer, the inner middle connective tissue, and from the side of perilymph - the inner layer of the epithelial cell

layer [4, 25]. Figure 1 shows a schematic view of the RWM structure. The middle layer is the most complex one. Structurally, it comprises fibrocytes, collagens, microfibrils, elastin and nerve ends [25]. The two outer layers consist of epithelial cells. The RWM thickness in mammals examined in the course of the experimental studies: a guinea pig, a rat, and a chinchilla varies from a few to dozens of μm [26, 27]. In humans, the RWM thickness varies from about 40 μm in the vicinity of its center, to about 70 μm on the fringes [26, 27]. Importantly, the structure and the anatomy of the RWM in animals is similar to humans [4]. This makes it possible to transfer the results of animal research to applications involving the human inner ear. The shape of the human RWM is close to circular, slightly elliptic: with the longer diameter equal to about 2.3 mm (1.8-3.2 mm) and the shorter diameter approximately 1.9 mm (1.4-2.4 mm) [29].

2.2. Steering MNPs across the RWM

RWM is characterized by semi-permeability [25, 26, 30]. It has been demonstrated that a number of substances as well as miniature objects are able to permeate RWM [27, 30]. These include: sodium ions, antiseptics, antibiotics, toxins, and, interestingly, even latex spheres with a diameter of about 1 μm [26, 30]. This is of key importance considering the drug delivery strategies employing MNPs. It has been confirmed that NPs placed on the outer surface of the RWM are able to permeate it crosswise in a specific time [4,25,27,30]. The effectiveness of RWM permeability by different substances as well as NPs is influenced by many factors including size, configuration, concentration and electrical charge of the substance and the NPs. In addition, the thickness and the condition of RWM should be taken into account [26, 30, 31]. Considering the three-layered nature of RWM, the outer layers will provide the greatest resistance to the NPs permeation through RW [30]. There are two ways of movement of NPs through the layers of epithelium cells: transcellular and paracellular transportation [30,31]. Figure 2 shows a schematic illustration of the two ways of NPs transportation through the layer of epithelium cells. When it comes to the middle layer, the NPs will move between the component structures (e.g. collagens, microfibrils,

elastin). Figure 3 shows the schematic of the NPs movement process through the middle connective layer. NPs placed on the outer surface of the RWM will permeate it over time, primarily via the phenomenon of diffusion [30]. At such a small object scale (20-100 nm) Brownian motion will also be significant [33], naturally assisting in the general phenomenon of diffusion. MNPs and their aggregates will move through RWM via paths offering the lowest mechanical resistance. Particular tissues can be penetrated by single MNPs and their aggregates up to specific sizes. Table 1 collects the information about the size (hydrodynamic diameter) of nanoparticles and their aggregates, which are able to cross the RWM barrier after being applied to its surface. The works [34,35] demonstrate that MNPs with a hydrodynamic diameter of up to 200 nm are able to cross e.g. epithelium cells. The study [36] provides results which indicate the clear influence of the NPs size of and the ability to penetrate RWM (diameter of NPs — 95 nm to 240 nm). Studies determining the size of the individual NPs can be used as grounds for arguing the size of the aggregates able to cross the RWM. In the conclusion to the work [4], it has been shown that NPs measuring from 10 to 640 nm are able to cross RWM. The work [28] presents the results of the experimental studies of movement of MNPs 300 nm in diameter through RWM. It has been clearly stated that there is an increase in the velocity of crossing RWM when using the external magnetic field. The study [32] demonstrates that epithelium cells can be penetrated by NP aggregates sized 200 — 400 nm. Additionally, it has been noted that aggregates of this size, most likely are coming from the layers of epithelium cells via paracellular transport. The work [20] demonstrates a clear influence of an external magnetic field acting on the MNPs sized 482.8 ± 158 nm, the MNPs crossed RWM within an hour, much faster than without the magnetic field. Furthermore, the works [34, 37] state that MNP aggregates with the average diameter of 770 nm were able to cross the barrier of epithelium cells assisted by the external magnetic field. The above-mentioned research results serve to confirm that objects less than 1000 nm in diameter, in particular below 750 nm, are able to cross RWM [26, 30, 34, 37]. Crossing RWM naturally (without additional stimuli to expedite the process) is time-consuming. It can

last anywhere from a few to dozens of hours. Using MNPs as micro-swarm drug carriers has the potential benefit of accelerating this process [13, 18]-[20]. In essence, the operating mechanism is the external magnetic field generating an extra pushing or pulling force to move the MNPs.

2.3. Forces acting on individual MNPs and their aggregates

The force necessary to displace a solid within a liquid of specific viscosity (drag force) may be calculated from the following formula (Stokes equation) [39]:

$$F_d = 6\pi R_{MNP}\eta\,\mathrm{u} \qquad (1)$$

where: F_d – drag force; R_{MNP} – radius of MNP (or aggregate); η – liquid viscosity; u – velocity. The pushing or pulling force for a single MNP (magnetic nanoparticle) or their aggregate generated by magnetic field should be equal to the drag force if achieving a specific velocity of the MNPs is desired. The magnetic force can be calculated from the equation below [39,40]:

$$F_m = \frac{2\pi R_{MNP}^3 \mu_0}{3} \cdot \frac{\chi}{1+\chi^3} \nabla H^2 \qquad (2)$$

where: F_m – magnetic force; μ_0 – permeability in free space; χ – volume susceptibility of the nanoparticle; H – magnetic field strength. As they move, nanoparticles will form aggregates in time. One of the main forces responsible for this phenomenon is the electrostatic force. The equation to calculate this force is provided, among others, in the work [39]:

$$F_e = \frac{2\pi\varepsilon_r\varepsilon_0 R_{MNP} s^2 \kappa e^{-\kappa s}}{1+e^{-\kappa s}} \qquad (3)$$

where: F_e – electrostatic force; κ – reciprocal double layer thickness; ε_r, ε_0 – relative and static permittivity of water; s – particle-particle separation distance. In addition, one can define a separate magnetic force of attraction of two adjacent particles. The formula to determine the value of this force is provided, among others, in the works [39,41]:

$$F_{md} = \frac{24\pi\mu_0 R_{MNP}^6 M_S^2}{9(s+2R_{MNP})^4} \qquad (4)$$

where: M_S - saturation magnetization.

The resultant of these forces together with the actual viscosity of the RWM material affects the condition of movement of MNP aggregates; in particular this applies to the average velocity of their motion.

2.4. The processes of MNPs aggregation

The process of aggregation of MNPs, along with the shape and size of the individual MNPs has a decisive influence on their magnetic properties [42]. These processes are very complicated at the level of detail. This is connected with the structure of MNPs with a magnetic core (e.g. Fe304) and its surrounding hydration layer [43]. Therefore, the process of aggregation is affected by two main groups of factors: chemical and physical (mechanical). The group of chemical factors includes the following features and phenomena: pH, valences, hydrated ionic radii, hydration layer and hydration forces [43]. On the other hand, the physical factors can include: magnetic attraction, electrostatic forces and specific ion effect of metal cations [43]. Drug delivery system designers employing MNPs try to eliminate as many factors affecting uncontrolled aggregation as possible, which may hinder MNP delivery. An example of such an action is coating the MNPs core with different substances. Such an approach can potentially eliminate the electrostatic attraction of MNPs, as was the case with dextran, for example [44, 45]. Due to the fact that dextran is non-ionic, the determined zeta-potential of such MNPs in a wide range of pH values is close to zero [44].

Single MNPs tend to quickly form larger aggregations. First, combinations of two MNPs (dimers) and three MNPs (trimers) are formed. Subsequently, chains of MNPs are formed, eventually leading to the formation of complex structures of different shape and varying size [34, 46, 47]. The study [47] provides conclusions from an experimental observation showing that the length of the aggregate chain is limited. It was noted that when the chain length exceeds 14 particles, the lateral aggregation accelerates. On the basis of this conclusion, it can be assumed that this process leads to a more rounded, ellipsoidal, in the ideal case – spherical aggregate shape.

2.5. Development of the numerical FEM model

Figure 4 presents a schematic overview of the FEM model development process. As a result of the additional force assisting the movement in RWM material (magnetic force F_M), single MNPs, and more often their aggregates, move through areas with the smallest resistance to movement (lowest viscosity). Consequently, an approach has been proposed to determine the value of the required magnetic force F_M effecting the movement of single MNPs and their aggregates in the medium with the specified viscosity value (average mock viscosity η_{ave}). For the purpose of the present paper, it has been assumed that the resistance force during motion of MNPs with a specific velocity in the medium with specific characteristics can be balanced with the magnetic force F_M. Therefore, once the resistance force value is known, it will be possible to determine the necessary parameters of the magnetic field to cause MNPs movement with a given velocity. In line with the assumptions, the material in which MNPs movement takes place has been modelled as an Eulerian body (element type EC3D8R). However, due to decisively higher rigidity in relation to the RWM material, MNPs have been modelled as a rigid Lagrangian body (element type C3D10M) for the purpose of FEM model calibration. The dimensional scale of the problem under consideration proves challenging for the development of a FEM model. The first step is to determine the effective size of the finite elements D_{FE} in the model. Afterwards, it must be determined which dimension of the RWM sample α_{RWM} in relation to the dimensional characteristic of the MNPs D_{FE} should be taken into account in order to obtain the calculation results within a reasonable time. For the purpose of model calibration, the movement of individual MNPs in a medium with known properties - the perilymphatic fluid - has been modelled. The determined viscosity value is η_{pf} = 0.86 mPa·s [19]. The used MNP diameter is 50 nm. The assumed movement velocity is v_M = 10 nm/s. The magnetic force value F_M, determined in the FEM analysis and required to effect the movement of MNPs with the specified velocity, was compared with the force value determined on the basis of the Stokes law. Calibration consisted of thickening the FEM grid in order to achieve a more accurate result and selecting an

acceptable degree of inaccuracy for the sake of achieving a reasonable calculation time. For the purposes of calibration, the dimension indicator I_D has been introduced, which connects the diameter of MNPs D_{MNP} and the characteristic dimension of the finite element D_{FE} :

$$I_D = \frac{D_{MNP}}{D_{FE}} \qquad (5)$$

At this stage of the research, the MNPs were placed in a cubic material sample with the side length 5 times greater than the MNP diameter. Table 2 shows the obtained results for the magnetic force value F_M from FEM analyses based on different values of the dimension indicator I_D. The next step was to determine the influence of the size of the RWM sample (α_{RWM}), in which the MNP occurs, together with its impact on the accuracy of the results and the time to obtain them. For the purpose of the present analysis, the RWM dimension indicator I_{RWM} was introduced, linking the dimension of the RWM sample - α_{RWM} and the MNPs D_{MNP}:

$$I_{RWM} = \frac{\alpha_{RWM}}{D_{MNP}} \qquad (6)$$

Tables 3 and 4 present the summary of the results of the magnetic force F_M calculation for different values of α_{RWM}. The analyses have been carried out for D_{MNP} = 50 nm and for two different D_{FE} values: 5 nm and 10 nm. The velocity and viscosity have remained unchanged. These results lead to the conclusion that a greater value of I_{RWM} does not necessarily lead to more accurate results. Therefore, the I_{RWM} value is of secondary importance. The most important characteristic is the dimension of the finite element D_{FE}. Based on this assertion, additional analysis has been carried out for the values: D_{MNP} = 50 nm, I_{RWM} = 2 and I_D = 25. The force value $F_{M\text{-}FEM}$ = 0.00392 fN, and the percentage difference is 3.72%. What follows is that a low value of I_{RWM} and a suitably high value of I_D = 25 may also produce accurate results. The last stage of the calibration of the FEM model was to determine the accuracy of determination of the force $F_{M\text{-}FEM}$ value with different sizes of MNPs (Table 5). These analyses can be useful in determining the MES model parameters for the aggregates of relatively large size (less than 750 nm) which

comprise MNPs of smaller sizes (e.g. 20 nm). It is therefore conclusive that controlling the parameters of I_{RWM} and I_D leads to satisfactory results. It is important insomuch as larger objects moving in areas with lower resistance to movement will utilize channels with a diameter not exceeding 1000 nm [26,30]. Analyses employing the Lagrangian-Eulerian approach are very time consuming. Using them to calculate the total time required for the movement of MNPs through RWM would be impossible. However, such method can still be of use in the current approach. It is sufficient to determine the values of the specified parameters of analysis (force, velocity, viscosity, etc.) in a sufficiently short time, enabling the stabilization of these parameters during calculations. The larger the object (this applies to both individual MNPs and their aggregates), the longer it takes to stabilize the parameters. For MNPs with the diameter of D_{FE} = 50 nm, the total time of analysis was t_A = 5 ns, whereas the time needed for the stabilization of the force value $F_{M\text{-}FEM}$ was t_{PS} = 2 ns. MNPs with the diameter D_{FE} = 750 nm, required a total analysis time of t_A = 150 ns,whereas the time required for the stabilization of the force value $F_{M\text{-}FEM}$ was t_{PS} = 60 ns.

3. Results

The present work analyzes the formation of aggregates which can be divided into two groups. The first group includes single-layer aggregates consisting of between a few and a few dozen MNPs. The second group applies to aggregates with a large number of MNPs, forming complex, solid shapes. In the first section two approaches to modelling the aggregate shapes have been proposed. In the second section the concept of average mock viscosity η_{ave} of RWM has been proposed together with determination of its value and demonstration of its utility.

3.1. Development of the MNP aggregate models

MNPs begin to form aggregates within a short time. The possible range of shapes is extremely varied. Considering their transportation through RWM, their maximum size will be limitedby the size of the natural passageways through RWM. In accordance with the information in section 2.2, the maximum dimension does not exceed 1000 nm and the majority of the literature sources confirms that MNPs and their aggregates with dimensions not exceeding 750 nm facilitate the most efficient transportation. Figure 5 shows the aggregate formation diagram. Assuming that the diameters of MNPs correspond to the hydrodynamic diameters of these particles, forming the aggregate entails them coming into contact. First, clusters of 2 and 3 particles are formed, and later they create more complex forms by merging together. First, one layer is formed (Figure 5e) and then more complex, solid structures are formed (Figure 5f). In the case of single-layer aggregates, it is possible to propose an algorithm for describing its shape. This is justified due to the simplification of assigning particular shapes of aggregates consisting of MNPs coated with specific substances which intend to arrest the process of aggregation. Consequently, small aggregates with simple shapes are formed, comprising between a few and a few dozen individual MNPs. The results of using such a substance has been presented in works [44, 45]. Figure 6 presents a way of describing the shape of single-layer aggregates, which can be useful when modelling them for the purpose of the FEM model construction. For example, the designation

1L(3)-5-1R(1) indicates that we are dealing with a 3-layer aggregate. The middle layer is the most numerous, comprising 5 singular MNPs; next, the 1L(3) stands for 1 MNP to the left of the middle layer is attached to 3 MNPs. Whereas 1R(1) denotes 1 MNP on the right side, attached to the first MNP of the middle layer. For larger three dimensional aggregates, the proposed formulation becomes too complicated to employ. However, aggregates consisting of dozens of MNPs form solids of irregular shapes by combining and partially permeating hydrational layers. The beginning of this process is shown in Figure 6c. Figs. 6c, 6d and 6e demonstrate examples of actual MNP aggregates.

For analyzing solid aggregates with complex shapes, the best solution is to build a three dimensional model that corresponds to the shape of the aggregate. Figure 7 shows the result of development of such a model based on microphotography [50]. There are therefore two scenarios for researching MNPs and their aggregates. In the case of simple single- layer structures, it is possible to use the proposed shape description algorithm. Whereas for more complex forms of solid aggregates, it is possible to develop their three dimensional models.

3.2. Determination of average mock viscosity η_{ave}

Viscosity is the primary parameter of liquids. Its exhibits a very broad range of possible values, eg. The viscosity of water at 25°C is η_w = 0.89 mPa·s, and the viscosity of tar (25°C) is η_t =1·10^7 Pa·s. From the biological perspective, RWM is an object composed of materials with different characteristics. It is assumed that intracellular viscosity is approximately 1 mPa·s [19,51]. However, the viscosity of the other constituents of the connective tissue, e.g. loose collagen matrix, is much higher and ranges from 8-13 Pa·s [19,52]. MNPs and their aggregates, provided their size is appropriate (diameter less than 750 nm), move through RWM along the path of the lowest mechanical resistance (lowest viscosity). Based on the results of experimental studies contained in the works [19, 28, 42] it is possible to determine the average mock viscosity of RWM as η_{ave}. The [42] concludes that the viscosity of RWM material should

be at least 1000 times greater than the viscosity of water. The exact value range can be determined on the basis of the information about the size of MNPs and the time of movement through RWM. The [19] determines the magnetic force value F_M enabling MNPs of the specified size to travel through the model RWM of the guinea pig in the course of one hour. In [28], the required magnetic force F_M value required for MNPs 300 nm in diameter to move through the RWM of the rat within one hour was determined. Table 6 summarizes the thickness values of RWM of the guinea pig and the rat available in various literature sources. The average thickness of the rat's RWM is approximately 13.75 μm, whereas for the guinea pig it is approx. 20 μm. According to [28], the magnetic force F_M with a value in the range from 0.3 fN to 1.2 fN facilitates an effective acceleration of MNP movement for particle diameters of 300 nm. After one hour, a large number of MNPs which have successfully crossed the RWM was observed. Of course, the transportation time by different particles was not the same, but it can be assumed that 1h constitutes the average time that is required. The results of the work [19] apply to MNP aggregates with a diameter from 50 nm to 130 nm crossing within 1h. The force F_M needed to facilitate this process was 0.651 fN. Assuming the thickness of the model RWM equal to the thickness of the guinea pig RWM, it is possible to determine the average mock viscosity of RWM as η_{ave}. These results can then be verified using the results provided in [28]. Table 7 contains the predicted values of average mock viscosity η_{ave} on the basis of the results of experimental studies presented in the works [19, 28]. The viscosity values were derived using the Stokes law. After accounting for the extreme RWM thickness values, it can be assumed that the average mock viscosity η_{ave} ranges between 0.0239 Pa·s and 0.1913 Pa·s.

3.3. FEM model verification using the results of experimental studies

The work [19] provides very interesting and valuable research results on the estimation of the magnetic force values F_M generated by the proposed arrangement of magnets. The values of these forces were used to estimate the velocity of the v_{agr}

aggregates with a diameter of $D_{A\text{-}MNP}$ = 50-130 nm, derived from MNPs with the diameter of 10 nm. The velocity value was estimated for the movement of aggregates in perilymphatic fluid with assumed viscosity value of η_{pf} = 0.855 mPa·s. Table 8 shows the value of the magnetic force F_M generated by individual magnets. It also provides the predicted velocities v_{agr} used as a basis for the FEM analysis carried out for the aggregate with a diameter of $D_{A\text{-}MNP}$ = 130 nm. The work [19] assumes a close to spherical shape of these aggregates.

Based on the photograph of PLGA particles as presented in Figure 8, the FEM model of the aggregates (A and B) has been developed and the analysis of their velocity has been carried out with the assumed magnetic force value F_M (magnet 3). Due to their irregular shape, velocities of the aggregates v_{agr} will be different for different directions of movement. To find the difference in their values, the analysis has been conducted along the four main directions: x, y, DS and DG. Figure 9 shows the discretized models of MNPs aggregates A and B. It also indicates the directions relative to which the velocity of the aggregate movement has been studied.Furthermore, the velocity of the aggregates in each such direction has been given. Estimation of MNPs velocity in a medium with a specific viscosity based on the Stokes law applies only to spherical shapes. If it were assumed that the aggregates A and B (Figure 8) were spheres with the diameter D_{SA} = 93 nm and D_{SB} = 100 nm, their velocities in perilymphatic fluid at the force 0.651 fN (magnet 3) would equal to v_A= 869 nm/s and v_B = 808 nm/s. When analyzing the velocity value of the aggregates in Figure 9, it is easy to notice significant differences in velocity values depending on the direction of movement. It can be clearly concluded that assuming the spherical shape for the purpose of simplification can in many cases lead to measurement errors.

3.4. Single-layer and spatial aggregates

For the purpose of this study, aggregates formed of MNPs with a diameter D_{MNP} = 50 nm have been chosen. Figures 10-13 show the obtained value of the magnetic force F_M which is required to maintain the movement velocity v_{agr} = 10 nm/s of selected

aggregates in a medium with the average mock viscosity η_{ave} from 0.0239 Pa·s to 0.1913 Pa·s. Such assumed velocity makes it possible to cross the rat RWM in less than 23 min, and less than 34 min for a guinea pig RWM. The value of the dimension indicator I_{RWM} fluctuated close to 2 (relative to each dimension of the aggregate). The D_{FE} value in each case was less than 15 nm. When analyzing the results shown in Figures 10-14, it can be concluded that the proposed method of calculating the magnetic force value F_M is effective for a wide range of viscosity values. The negative side of the employed method is the significant increase in the calculation time as the viscosity value increases. However, for a given shape at the assumed velocity, a linear increase in the value of viscosity appears to effect a linear increase in the value of the required magnetic force F_M. Based on this assumption, it is possible to perform calculations for smaller viscosity values and re-calculate the value of the magnetic force F_M for higher values. The presented results confirm the validity of the above mentioned assumption, because the ratio of the calculated values of magnetic forces F_M does not deviate from the ratio of the average mock viscosity η_{ave} by more than 5.5%. In addition, the value of magnetic forces F_M has been calculated for the spatial aggregates in Figure 7. The parameters of the analysis were similar to single-layer aggregates. The calculation was performed for a single designated direction of movement. The obtained results confirm the feasibility of analyzing any aggregate shape (Figures 14-15). When modelling the spatial aggregate, its faithful recreation is of crucial importance, both in the stage of creating a solid model, and afterwards when breaking an object into finite elements.

4. Discussion

The topic of precise drug delivery to the inner ear using MNPs is extremely complex. RWM is characterized by semi-permeability, therefore objects with a diameter of less than 1000 nm are able to cross it. Based on the results of the research presented in subject literature, it can be concluded that in order to freely cross the blood-perilymph barrier, the MNPs and their aggregates should not be larger than 500 nm — 750 nm. Most scientists estimate the movement parameters of individual MNPs using the

Stokes law. The major limitation of this method is the fact that that it only allows for the analysis of spherical objects. Figure 9 illustrates the scale of possible differences in the estimated velocity value of MNPs for shapes that are actually irregular. This is despite that fact that analyzed aggregates were close to spherical. Another issue was the viscosity value assumed during the analysis. An important aid when analyzing the processes of MNPs crossing the RWM is the proposed average mock viscosity η_{ave}. In accordance with the presented calculations based on the results of the experimental research presented in selected publications, it can be concluded that the average mock viscosity η_{ave} value is between 28 and 222 times higher than the viscosity of perilymphatic fluid. The method presented in this work makes it possible to precisely determine the movement parameters of magnetic aggregates of any shape in the medium with a specific viscosity. In connection with different ways of reducing the aggregation process, the aggregates can be analyzed in two ways. Single-layer aggregates can be accurately described using the proposed algorithm. This can be helpful in the case of MNPs coated with substances intended to arrest the process of aggregation. In turn, large spatial aggregates can be analyzed as solid objects with external dimensions corresponding to the dimensions of the hydrodynamic aggregate. The determined value of the average mock viscosity η_{ave} presented in this study can also be helpful in the simplified analysis of transport of MNPs through RWM.

5. Conclusion

Treatment of the inner ear disorders poses a challenge both due to anatomical and physiological barriers of the ear. The anatomic inaccessibility of the inner ear coupled with poor penetration through the blood-perilymph barrier and permeation of drug molecules through RWM results in sub-therapeutic concentrations of the drug at the site of action. In this work, we present a methodology for the evaluation of the magnetic forces needed to move magnetic particles and their aggregates through the cochlea round window membrane for efficient intracochlear drug delivery. To our knowledge the employment of the Lagrangian-Eulerian method to describe the penetration of

magnetic nanoparticles guided by magnetic fields through the RWM has not yet been addressed**.** The main advantage of the proposed FEM methodology is that it allows the simulation of aggregates of particles with different shapes and sizes instead of only spherical objects. The analysis of the predictive magnetic force results complement the magnetically guided drug delivery experiments, both in-vitro and in-vivo, which were published earlier. These simulation findings hold a great potential to improve the penetration capabilities of MNPs used for drug delivery into the cochlea [60],[61]. Further experimental work using the presented methodology could make it possible to further clarify the value of the average viscosity η_{ave} with regard to RWM.

Funding

This work was supported by the French Programme: Plan Cancer 2014-2019, Inserm, Project: Microrobots Targeting Glioblastoma. With financial support received from ITMO Cancer AVIESAN (Alliance Nationale pour les Sciences de la Vie et de la Santé, National Alliance for Life Science & Health) within the framework of the Plan Cancer initiative.

Conflict of Interest

The authors declare no conflict of interest was present. The funders had no influence over the preparation of the study, the collection, analyses, or interpretation of data herein as well as on in the writing of the present manuscript as well as on the decision to publish the results.

References

1. Caroline Guigou , Alain Lalande, Nadine Millot, Karim Belharet and Alexis Bozorg Grayeli, , "Use of Super Paramagnetic Iron Oxide Nanoparticles as Drug Carriers in Brain and Ear: State of the Art and Challenges" *Brain Sciences*, **2021**, 11, 358.
2. Shapiro B, Kulkarni S, Nacev A, Sarwar A, Preciado D, Depireux DA. "Shaping magnetic fields to direct therapy to ears and eyes" *Annu Rev Biomed Eng* **2014**;16:455–81
3. Rahul Mittal et al. , "Nanoparticle-based drug delivery in the inner ear: current challenges, limitations and opportunities", *Artificial Cells, Nanomedicine, And Biotechnology***, 2019**, Vol. 47, No. 1, 1312–1320
4. F. Valente et al., "Nanoparticle drug delivery systems for inner ear therapy: An overview", *Journal of Drug Delivery Science and Technology*, **2017**, Vol. 39, pp. 28-35.
5. J. D. Fisher et al., "Micro and nanoparticle drug delivery systems for preventing allotransplant rejection", **2015**, *Clinical Immunology*, Vol. 160, pp. 24-35.
6. L. Mellal et al., "Modeling of Optimal Targeted Therapies using Drug-Loaded Magnetic Nanoparticles for the Liver Cancer" *IEEE Tran. on NanoBioscience*, **2016**, vol. 15 pp. 265-274.
7. A. Komaee, "Feedback Control for Transportation of Magnetic Fluids With Minimal Dispersion: A First Step Toward Targeted Magnetic Drug Delivery", *IEEE Transactions On Control Systems Technology*, **2017**, Vol. 25, No. 1, pp. 129-144.
8. Laura Sumner, Jonathan Mestel and Tobias Reichenbach1 "Steady streaming as a method for drug delivery to the inner ear", *Scientific Reports*, **2021**, 11:57.
9. Ai-Ho Liao et al. "Ultrasound-induced microbubble cavitation via a transcanal or transcranial approach facilitates inner ear drug delivery", *JCI Insight.* **2020**, 5(3), e132880.
10. G. Chen, et al.,"Disposition of nanoparticle-based delivery system via inner ear administration", *Curr. Drug Metab.*, **2010**, Vol. 11, pp. 886-897.
11. Y. Malam, et al., „Liposomes and nanoparticles: nanosized vehicles for drugdelivery in cancer, *Trends Pharmacol. Sci.,* **2009**, Vol. 30, pp. 592-599.
12. S. Gelperina, et al., „The potential advantages of nanoparticle drug delivery systems in chemotherapy of tuberculosis", *Am. J. Respir. Crit. Care Med.* **2005**, Vol. 172, pp. 1487-1490.
13. K. J. Dormer et al., Magnetically-Targeted, Technetium 99m-Labeled Nanoparticlesto the Inner Ear", *Journal of Biomedical Nanotechnology*, **2008**, Vol. 4, Number 2, pp. 174-184.
14. A. Mahmood et al., "A Novel Design of an MPI-Based Guidance System for Simultaneous Actuation and Monitoring of Magnetic Nanoparticles", *IEEETransactions On Magnetics*, **2015**, Vol. 51, No. 2.
15. M. D. Tehrani et al., "A Novel Scheme for Nanoparticle Steering in Blood Vessels Using a Functionalized Magnetic Field" *IEEE Trans. on Biomedical Engineering*, **2015**, Vol. 62, No. 1.
16. Z. G. Forbes et al., "Validation of High Gradient Magnetic Field Based Drug Deliveryto Magnetizable Implants Under Flow", *IEEE Transactions on Biomedical Engineering*, **2008**, Vol. 55, No. 2, pp. 643-649.
17. Y. Cui et al., "Enhanced intracellular delivery and controlled drug release of magnetic PLGA nanoparticles modified with transferrin" *Acta Pharmacologica Sinica*, **2017**, Vol. 38, pp. 943-953.

18. X. Du et al., "Magnetic Targeted Delivery of Dexamethasone Acetate Across the Round Window Membrane in Guinea Pigs", Otology & Neurotology, **2013**, Vol. 34(1), pp. 41-47.
19. A. L. Barnes et al., "Magnetic characterization of superparamagnetic nanoparticles pulled through model membranes" *BioMagnetic Research and Technology*, **2007**, Vol. 5.
20. M. Thaler, et al., "Visualization and analysis of superparamagnetic iron oxide nanoparticles in the inner ear by light microscopy and energy filtered TEM. *Nanomedicine: NBM*, **2011**, Vol. 7, pp. 360-369.
21. K. Talaśka, A. Ferreira, "An Approach to Identifying Phenomena Accompanying Micro and Nanoparticles in Contact With Irregular Vessel Walls", *IEEE Transactions on NanoBioscience*, **2017**, Vol. 16, No. 6, pp.463-475.
22. T. K. Malherbe et al., "Constructing a three-dimensional electrical model of a living cochlear implant user's cochlea", *Int. J. Numer. Meth. Biomed. Engng.*, **2016**, e02751.
23. M. Mehdi et al., "A Linked Data Visualiser for Finite Element Biosimulations", *International Journal of Semantic Computing*, **2016**, Vol. 10, pp. 219-245.
24. V. Gylienė et al., "Vibrational and numerical evaluation of human incus mechanical properties", MECHANIKA, **2016**, Volume 22, pp. 525-529.
25. I. Pyykkö et al., "Nanoparticle based inner ear therapy", *World J Otorhinolaryngol*, 2013, Vol. 3(4), pp. 114-133.
26. D. Mao-li et al., „Permeability of round window membrane and its role for drug delivery: our own findings and literature review", *Journal of Otology*, **2009**, Vol. 4, No. 1, pp. 34-43.
27. N. El. Kechai, et al., "Recent advances in local drug delivery to the inner ear", *International Journal of Pharmaceutics*, **2015**, Vol. 494, pp. 83-101.
28. A. Sarwar et al., "Magnetic Injection of Nanoparticles Into Rat Inner Ears at a Human Head Working Distance", IEEE Transactions on Magnetics, **2013**, Vol. 49, No. 1, pp. 440-452.
29. Y. Nomura, "Otological significance of the round window", *Adv Otorhinolaryngol*, **1984**, Vol. 33, pp. 1-162.
30. M. V. Goycoolea, L. Lundman, „Round Window Membrane. Structure Function and Permeability: A Review", *Microscopy Research and Technique*, **1997**, Vol. 36, pp. 201-211.
31. J. Zou et al., "Efficient penetration of ceric ammonium nitrate oxidant-stabilized gamma-maghemite nanoparticles through the oval and round windows into the ratinner ear as demonstrated by MRI", *J Biomed Mater Res Part B*, **2017**, Vol. 105B, pp. 1883-1891.
32. V. Konstantinova et al., "Nano-TiO2 penetration of oral mucosa: in vitro analysis using 3D organotypic human buccal mucosa models", *J Oral Pathol Med*, **2017**, Vol. 46, pp. 214-222.
33. B. Uma et al., "Nanoparticle Brownian motion and hydrodynamic interactions in the presence of flow fields", *Physics of Fluids*, **2011**, Vol. 23, 073602 (1-15).
34. A. K. Hoshiar et al., "Studies of aggregated nanoparticles steering during magnetic-guided drug delivery in the blood vessels", Journal of Magnetism and Magnetic Materials. **2017**, Vol. 427, pp. 181-187.
35. J.V. Georgieva, et al., "Surface characteristics of nanoparticles determine their intracellular fate in and processing by human blood-brain barrier endothelial cells in vitro", *Mol. Ther.*, **2011**, Vol. 19/(2), pp. 318-325.
36. J. Zou et al., "Size-dependent passage of liposome nanocarriers with preserved post

transport integrity across the middle-inner ear barriers in rats", *Otol Neurotol.*, **2012**, Vol. 33(4), pp. 666-673.

37. T.D. Do, e al., "Guidance of magnetic nanocontainers for treating alzheimer's disease using an electromagnetic, targeted drug delivery actuator", *J. Biomed. Nanotechnol.*, **2016**, Vol. 12/(3), pp. 569–574.
38. K.M. Pondman, et al., "Magnetic drug delivery with FePd nanowires, J. Magn. Magn. Mater.", **2015**, Vol. 380, pp. 299-306.
39. X. Gao, et al., "Magnetic Assisted Transport of PGA Nanoparticles Through a Human Round Window Membrane Model", Journal of Nanotechnology in Engineering and Medicine, **2010**, Vol. 1, pp. 031010-1-031010-6, August.
40. B. Shapiro, et al., "Control to Concentrate Drug-Coated Magnetic Particles, to DeepTissue Tumors for Targeted Cancer Chemotherapy." Proceeding, of the 46th IEEEConference on Decision and Control. **2007**, Vol. 46. pp. 3901-3906,
41. R. A Wassel.., B. P. Grady, R. D. Kopke, K. J. Dormer, "Dispersion of Super Paramagnetic Iron Oxide Nanoparticles in Poly(D,L-Lactide-co Glycolide) Microparticles," Colloids Surf.. A, **2007**, 292. pp. 125-130
42. J. M. Rojas et al., "Time-course assessment of the aggregation and metabolization of magnetic nanoparticles", *Acta Biomaterialia*, **2017**, Vol. 58 pp. 181-195.
43. H. Wang, et al., "Effects of monovalent and divalent metal cations on the aggregation and suspension of Fe3O4 magnetic nanoparticles in aqueous solution", *Science of the Total Environment*, **2017**, Vol. 586, pp. 817-826.
44. Ch. Ravikumar, et al., "Aggregation of dextran coated magnetic nanoparticles in aqueous medium: Experiments and Monte Carlo simulation", *Colloids and SurfacesA: Physicochem. Eng. Aspects*, **2012**, Vol. 403, pp. 1-6.
45. Y.W. Jun, et al. "Chemical design of nanoparticle probes for high performance magnetic resonance imaging", *Angew. Chem. Int. Ed.* **2008**, Vol. 47, pp. 5122- 5235.
46. D. Heinrich, et al., "Effects of magnetic field gradients on the aggregation dynamicsof colloidal magnetic nanoparticles", *Soft Matter*, **2015**, Vol. 11, pp. 7606-7616,.
47. J. Faraudo, J. Camacho, "Cooperative magnetophoresis of superparamagnetic colloids: theoretical aspects", *Colloid Polym Sci*, **2010**, Vol. 288, pp. 207-215.
48. Abaqus Documentation, **2017**.
49. J. Landers, et al., "Simultaneous Study of Brownian and Néel Relaxation Phenomena in Ferrofluids by Mössbauer Spectroscopy", *Nano Lett.*, **2016**, Vol.16 (2), pp. 1150-1155.
50. X. Ge, et al., "Distribution of PLGA nanoparticles in chinchilla cochleae", *Otolaryngology–Head and Neck Surgery*, **2007**, Vol. 137, pp. 619-623.
51. K. Fushimi, A. S. Verkman, "Low viscosity in the aqueous domain of cell cytoplasm measured by picosecond polarization microfluorimetry", *J Cell Biol*, **1991**, Vol. 112(4), pp. 719-725.
52. R. W. Chan, I. R. Titze, "Viscosities of implantable biomaterials in vocal fold augmentation surgery", *Laryngoscope*, **1998**, *Vol.* 108(5), pp.725-731.
53. A. A. Mikulec et al., "Permeability of the Round Window Membrane is Influenced by the Composition of Applied Drug Solutions and by Common Surgical Procedures" **2008**.

54. L. Nordang et al., "Morphologic changes in the round window membrane after topical hydrocortisone and dexamethasone treatment", *Otology and Neurotology*, **2003**, Vol. 24, pp. 339-343.
55. Tanaka K, Motomura S., "Permeability of the labyrinthine window in guinea pigs", *Arch Otorhinolaryngol*, **1981**, Vol. 233, pp. 67–75.
56. R. Z. Gan, "Dynamic Properties of Round Window Membrane in Guinea Pig Otitis Media Model Measured with Electromagnetic Stimulation", *Hear Res.*, **2013**, Vol. 301, pp. 125-136.
57. S. Hellström et al., "Structure of the round window membrane". *Acta Otolaryngol Suppl.* **1989**, Vol. 457, pp. 33-42.
58. A. Saber et al. "Middle ear application of a sodium hyaluronate gel loaded withneomycin in a Guinea pig model", *Ear Hear*, **2009**, Vol. 30, pp. 81-89.
59. H. Takeda et al., "Protein transduction therapy into cochleae via the round windowniche in guinea pigs", *Molecular Therapy — Methods & Clinical Development*, **2016**, Vol. 3, pp. 16055.
60. Gaëlle Leterme et al. "Superparamagnetic Nanoparticle Delivery to the Cochlea Through Round Window by External Magnetic Field: Feasibility and Toxicity", *Surgery Innovation*, **2019** Dec; 26(6):646-655.
61. Rathnam C, Chueng S-TD, Ying Y-LM, Lee K-B and Kwan K, "Developments in Bio-Inspired Nanomaterials for Therapeutic Delivery to Treat Hearing Loss". *Front. Cell. Neurosci.*, **2019**, 13:493.

Tables

Table 1: The sizes of NPs and their aggregates that are able to cross the barrier of RWM.

The diameter of NPs and their aggregates	Reference
200 nm	[35,38]
95 nm – 240 nm	[36]
300 nm	[28]
200 nm – 400 nm	[32]
10 nm – 640 nm	[4]
324.5 nm – 640.8nm	[18]
770 nm	[34,37]
1000 nm	[26,30]

Table 2: Comparison of the magnetic forces obtained for various values of the dimension indicator I_D, $F_{M\text{-}S}$ – magnetic force derived from the Stokes law, $F_{M\text{-}FEM}$ – magnetic force derived using FEM analysis.

Dimension indicator I_D	Force $F_{M\text{-}S}$ [fN]	Force $F_{M\text{-}FEM}$ [fN]	Percentage difference [%]	CPU time[s]
2	0.00405	0.0052	22.1	11.2
5	0.00405	0.00417	2.81	25
6.66	0.00405	0.00397	2.08	53.4
10	0.00405	0.00394	2.86	204.4
20	0.00405	0.00395	2.6	4479

Table 3: Comparison of magnetic force values obtained for different dimension indicators I_{RWM}, D_{MNP} = 50 nm, D_{FE} = 5 nm, I_D = 10.

Dimension indicator I_{RWM}	Force $F_{M\text{-}S}$ [fN]	Force $F_{M\text{-}FEM}$ [fN]	Percentage difference [%]	CPU time[s]
3	0.00405	0.00366	9.69	66.7
5	0.00405	0.00394	2.78	204.4
7	0.00405	0.00407	0.43	524.5
9	0.00405	0.0041	1.17	1157.4

Table 4: Comparison of magnetic force values obtained for different dimension indicators I_{RWM}, D_{MNP} = 50 nm, D_{FE} = 10 nm, I_D = 5.

Dimension indicator I_{RWM}	Force $F_{M\text{-}S}$ [fN]	Force $F_{M\text{-}FEM}$ [fN]	Percentage difference [%]	CPU Time [s]
3	0.00405	0.00385	5.0	23.1
5	0.00405	0.00417	2.9	25.0
7	0.00405	0.00429	5.86	55.5
9	0.00405	0.00433	6.84	89.6

Table 5: Verification model information: $F_{M\text{-}S}$ – value of the magnetic force derived from the Stokes law, $F_{M\text{-}FEM}$ – value of the magnetic force derived using FEM analysis.

D_{MNP} [nm]	Force $F_{M\text{-}S}$ [fN]	Force $F_{M\text{-}FEM}$ [fN]	Percentage difference [%]	I_{RWM}	I_D	CPU time [s]
20	0.00162	0.00153	5.6	5	10	225.3
50	0.00405	0.00394	2.8	5	10	204.4
100	0.0081	0.00740	8.7	3	16.67	832.8
250	0.0203	0.0194	4.7	3	16.67	1169.4
500	0.0405	0.0396	2.3	2	33.33	6791.4
750	0.0608	0.0597	1.8	2	39.47	10365.3

Table 6: Thickness of RWM in rats and guinea pigs.

Rat RWM thickness T_R [μm]	Source	Guinea pig RWM thickness T_{GP} [μm]	Source
12	[53,54]	10-30	[53,55]
11.5	[56]	10	[25,58]
15	[25,57]	25-30	[42]
16	[28]	~20	[59]

Table 7: Average mock viscosity values.

MNP diameter - D_{MNP} [nm]	Magnetic force F_M [fN]	Average thickness of RWM [μm]	Viscosity η_{ave} [Pa·s]
130	**0.651**	**20 ave**	**0.0956**
130	0.651	10	0.1913
130	0.651	30	0.0638
300	**0.3**	**13.75 ave**	**0.0278**
300	0.3	11.5	0.0332
300	0.3	16	0.0239
300	**1.2**	**13.75 ave**	**0.111**
300	1.2	11.5	0.1329
300	1.2	16	0.0955

Table 8: Values of magnetic forces generated by the magnets [19].

Magnet	Forcevalue F_M [fN]	Predicted velocity v_{agr} [nm/s]	Force $F_{M\text{-}FEM}$ [fN]	Percentage difference [%]
1	0.572	546	0.556	2.8
2	0.554	529	0.539	2.71
3	0.651	622	0.634	2.61
4	0.504	481	0.49	2.78

FIGURES

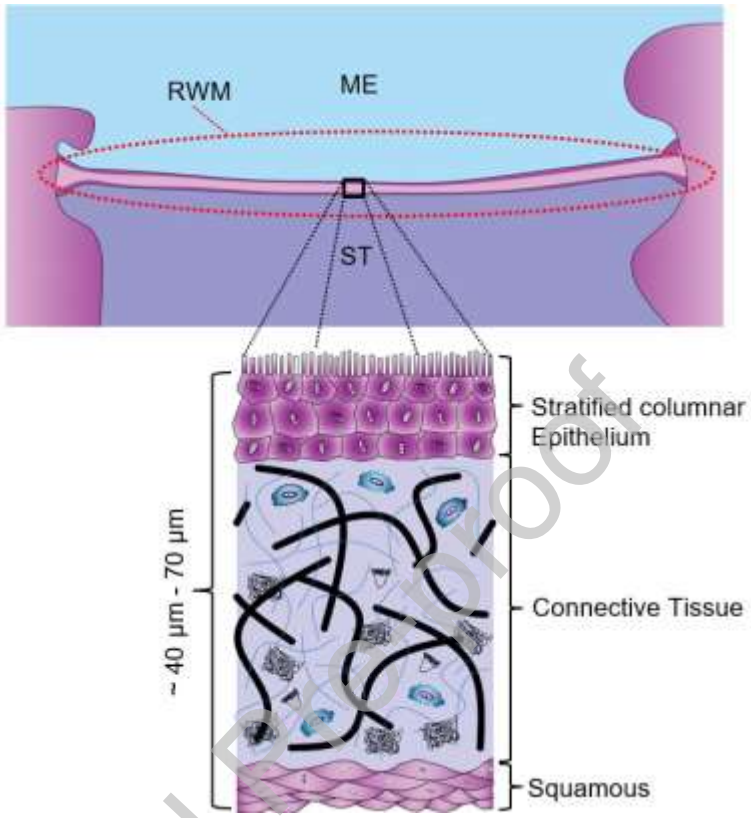

Figure 1: Structure of the round window membrane: ME – middle ear, ST – scala tympani, connective tissue: fibrocytes, collagens, microfibrils, elastin and nerve ends.

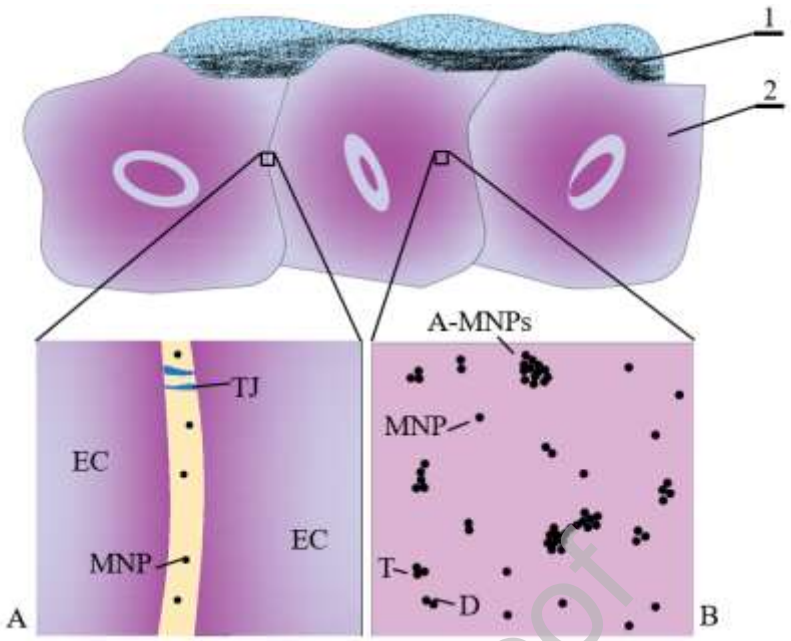

Figure 2 : Process of MNPs movement through the layers of epithelium cells: 1 – drop of gel with MNPs, 2 - epithelium cell — EC, TJ — tight junction, MNP — magnetic nanoparticle, A-MNPs – aggregates of magnetic nanoparticles, A – paracellular transport of MNPs, B – transcellular transport of MNPs, D – dimer, T – trimer.

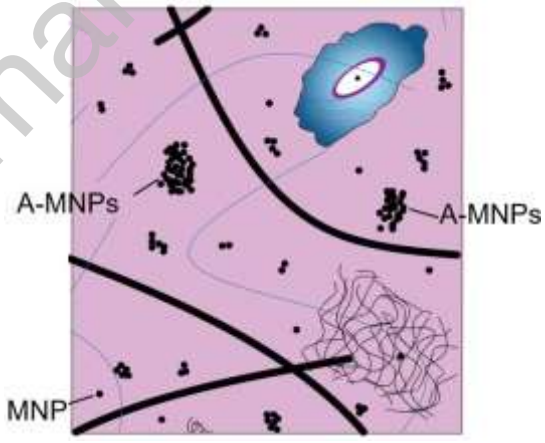

Figure 3 : The process of MNPs movement through the middle connective layer.

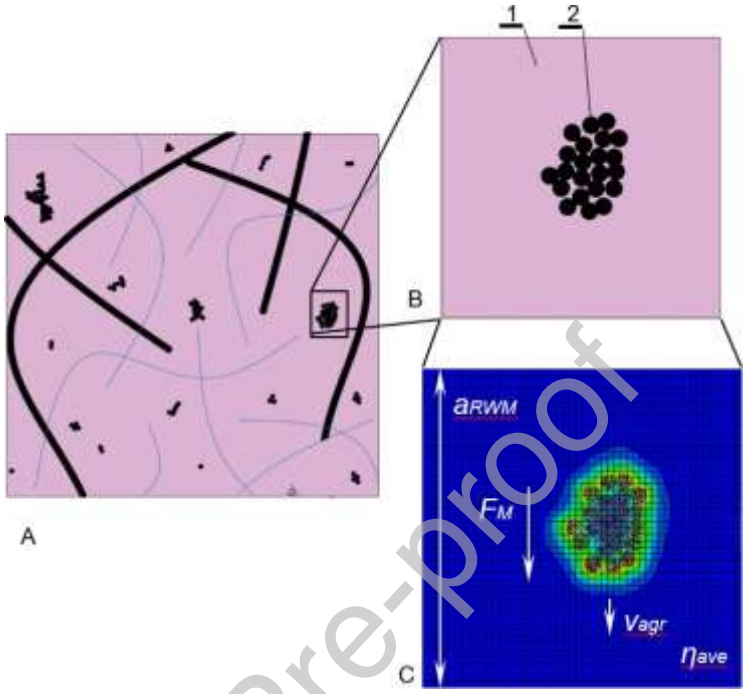

Figure 4 : Diagram of the numerical FEM model: A – RWM sample, B – close up of a selected MNPs aggregate, C – FEM model, 1 – Eulerian body, 2 – Lagrangian body, *FM* – magnetic force enforcing movement, *vagr* – aggregate velocity, *ηave* – average mock viscosity.

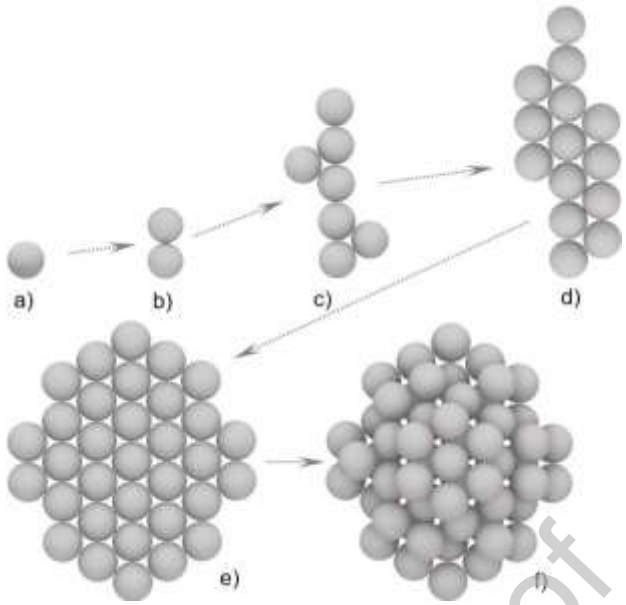

Figure 5 : Process diagram of aggregate formation from MNPs: a – e – single-layer aggregates, f — spatial aggregate.

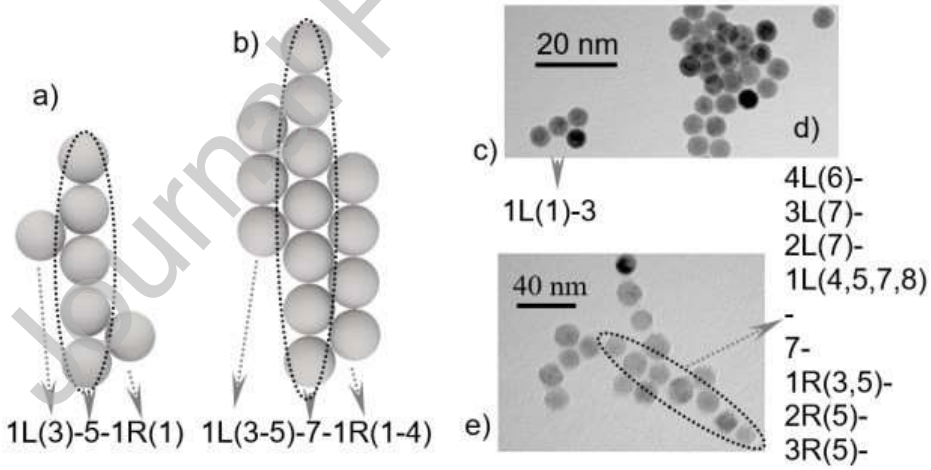

Figure 6: The description algorithm for a single-layer MNPs aggregate: a, b – model shapes, c – actual aggregate [49], d – actual spatial aggregate [49], e – actual aggregate [49].

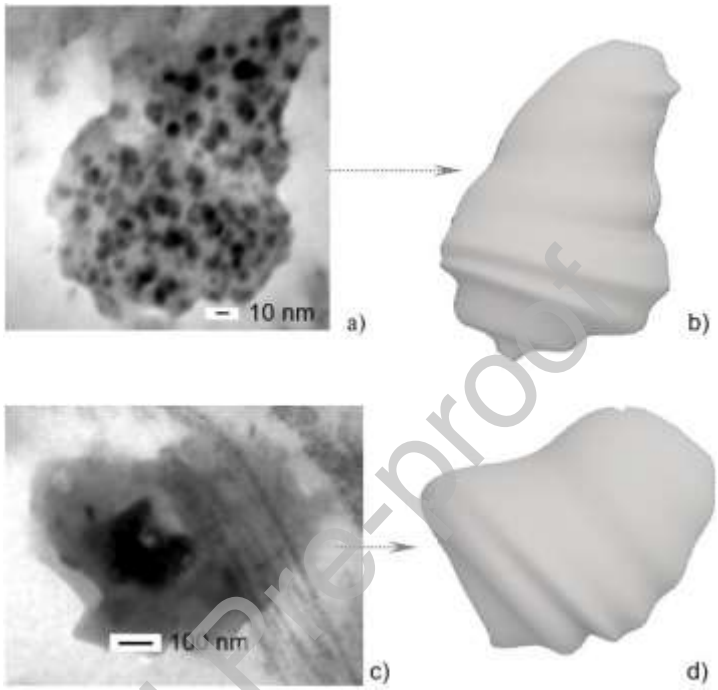

Figure 7: Development of the models mapping the shape of the MNPs aggregate: a - MNPs aggregate [48], b - solid model, c - MNPs aggregate [48], d - solid model.

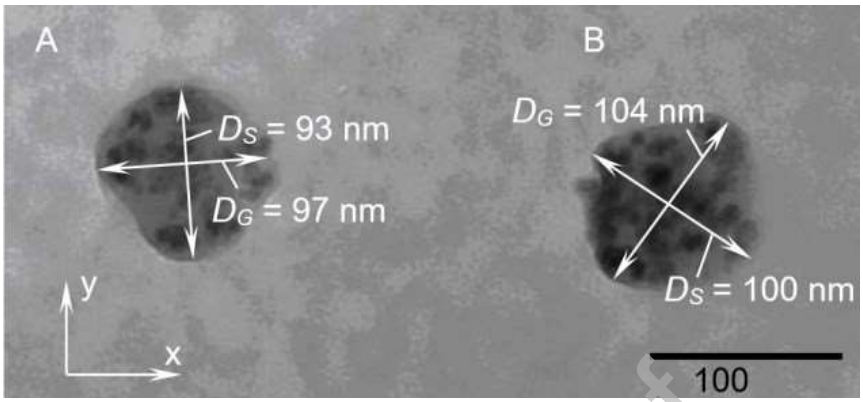

Figure 8: Microphotography of the PLGA particles [17]: DG – larger diameter, DS – smaller diameter.

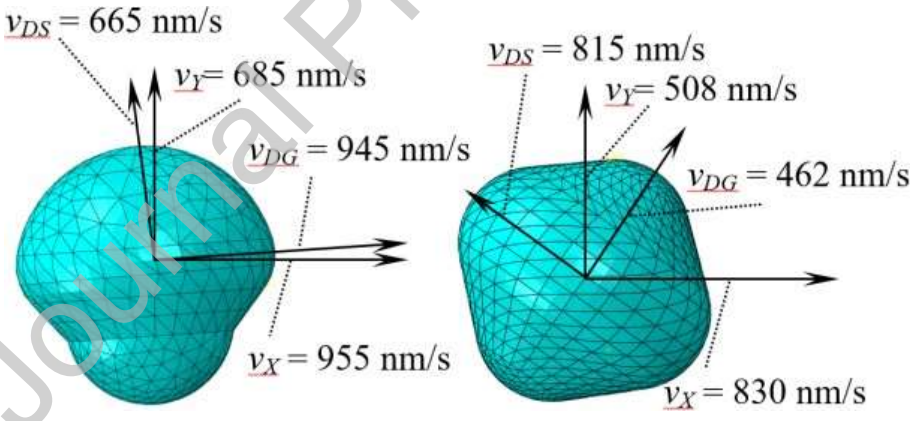

Figure 9: Discretized models of aggregates A and B.

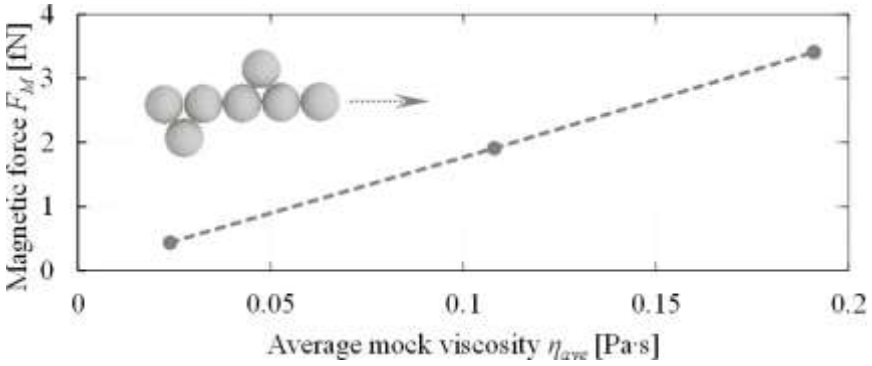

Figure 10: Value of the magnetic force F_M for the aggregate 1L(3)-5-1R(1) in the function of the average mock viscosity η_{ave}, arrow – direction of movement.

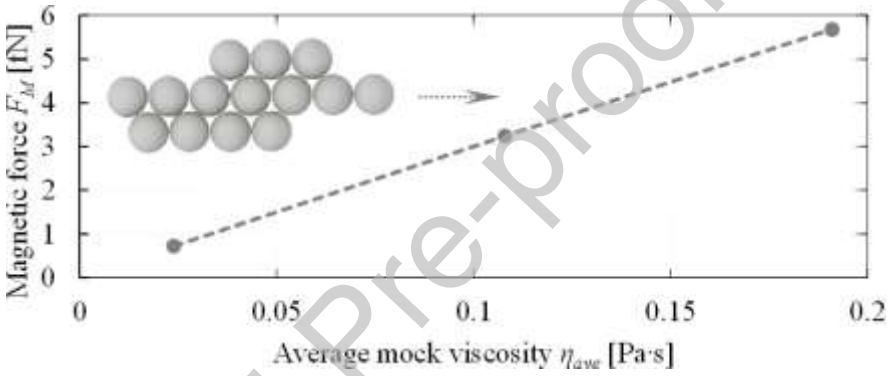

Figure 11: Value of the magnetic force F_M for the aggregate 1L(3-5)-7-1R(1-4) in the function of the average mock viscosity η_{ave}, arrow – direction of movement.

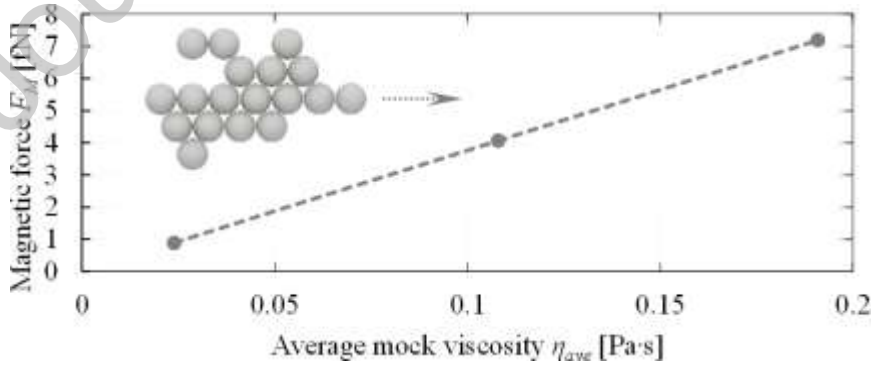

Figure 12: Value of the magnetic force F_M for the aggregate 2L(1-2,4)-1L(3-5)-7-1R(1-4)-2R(1) in the function of the average mock viscosity η_{ave}, arrow – direction of movement.

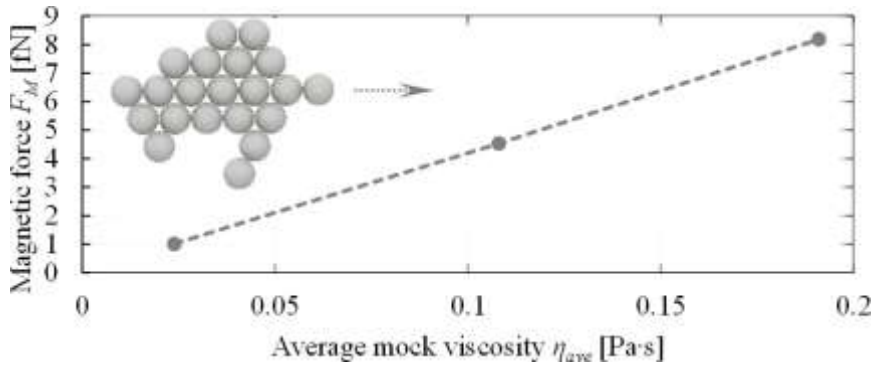

Figure 13: Value of the magnetic force F_M for the aggregate 2L(3,4)-1L(3-5)-7-1R(1-5)-2R(1,4)-3R(3) in the function of the average mock viscosity η_{ave}, arrow — direction of movement.

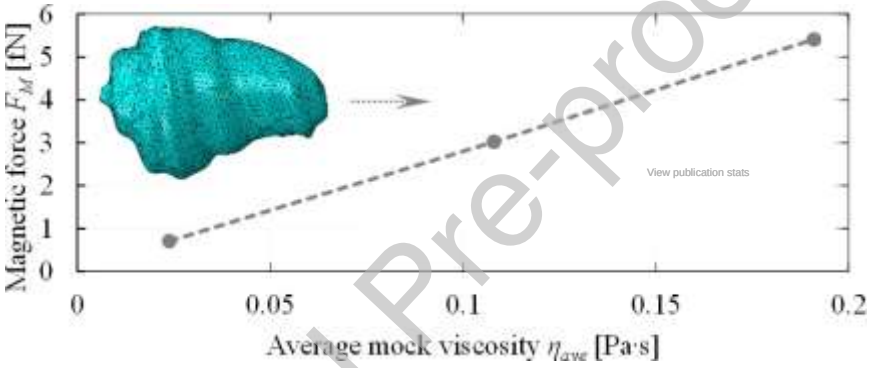

Figure 14: Value of the magnetic force FM for the aggregate from Figure 7a,b in the function of the average mock viscosity η_{ave}, arrow – direction of movement.

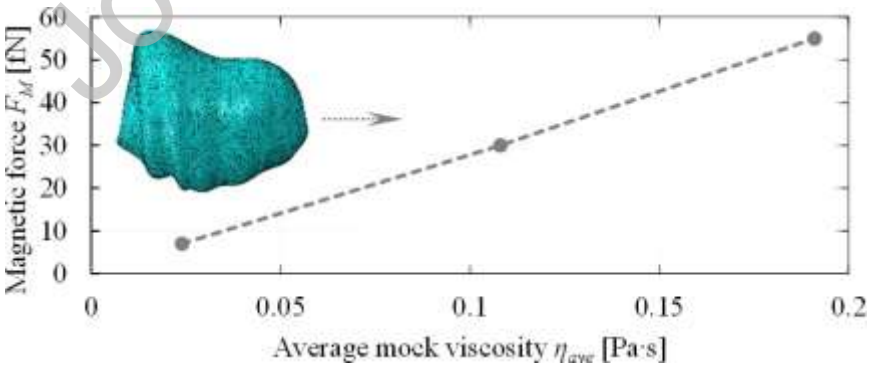

Figure 15: Value of the magnetic force F_M for the aggregate from Figure 7c,d in the function of the average mock viscosity η_{ave}, arrow – direction of movement.